

<sup>1</sup>Department of Atmospheric Sciences, Texas A&M University, College Station, Texas

<sup>2</sup>Forecast System Lab, National Oceanic and Atmospheric Administration, Boulder, Colorado

<sup>3</sup>North Carolina State University, Raleigh, North Carolina

## Numerical simulations of a large-amplitude mesoscale gravity wave event

F. Zhang<sup>1</sup>, S. E. Koch<sup>2</sup>, and M. L. Kaplan<sup>3</sup>

With 18 Figures

Received August 28, 2000; revised May 2002; accepted October 8, 2002

Published online: April 10, 2003 © Springer-Verlag 2003

### Summary

Numerical simulations with the NCAR/PSU Mesoscale Model 5 (MM5) were performed to study a large-amplitude gravity wave event that occurred on 4 January 1994 along the East Coast of the United States. Results from the MM5 control simulation using a 12-km mesh resolution compared well with the synoptic and mesoscale observational analysis. The simulated gravity waves displayed timing, location, wavelength, and propagation speed similar to those observed in a synoptic-scale environment described by the Uccellini and Koch (1987) conceptual model. Additional features existing upstream of the wave generation region not contained within their conceptual model were a warm occlusion and tropopause fold prior to and during the gravity wave generation. Wave ducting criteria were nearly satisfied along the path of the gravity waves.

Several sensitivity tests were performed. In a simulation in which the Appalachian Mountains were removed, the model still produced similar cyclone development and mesoscale gravity waves. Thus topography was not directly responsible for the gravity wave genesis. Also, three different “fake dry” sensitivity tests were performed with the latent heating related to changes of water substance turned off in the model at different stages of the simulation. The results from these simulations suggest that diabatic heating played an important role in both jet/cyclone development and in gravity wave amplification and maintenance, though not wave generation. The simulation with grid resolution increased to 4 km, which included fully explicit microphysics produced gravity wave characteristics similar to those in the control simulation, though the higher resolution resolved much shorter waves (though unverifiable) closely associated with convection.

This 4-km sensitivity experiment with no cumulus parameterization also confirmed that the dominant gravity wave was not an artifact of the particular cumulus parameterization scheme used for the control simulation. The reliability of the simulated gravity waves is further confirmed with another sensitivity experiment initialized ~20 hours before the observed wave generation in which qualitatively-similar gravity waves were produced.

### 1. Introduction

Mesoscale gravity waves have fascinated meteorologists because of their impact on the weather and their close association with extratropical cyclones (Brunk, 1949; Tepper, 1954; Ferguson, 1967; Bosart and Cussen, 1973; Eom, 1975; Uccellini, 1975; Stobie et al, 1983; Pecnick and Young, 1984; Bosart and Sanders, 1986; Koch and Golus, 1988; Lin and Goff, 1988; Schneider, 1990; Ralph et al, 1993 a, b; Koch and O’Handley, 1997; Bosart et al, 1998). These waves typically have wavelengths of 50–500 km, periods of 0.5–4 h, amplitudes of 0.5–15 hpa, and phase velocities of 15–35 m s<sup>-1</sup>. They are capable of organizing precipitation into bands, creating damaging winds, sleet and blizzard conditions, and triggering instabilities that lead to the development of severe convection.

Uccellini and Koch (1987), after surveying 13 cases of mesoscale gravity waves in the literature, found that such waves frequently appear in the vicinity of jet streaks and within the cool side of a surface warm or stationary front. They suggested that mesoscale gravity waves are generated as an upper-level jet streak propagates away from the geostrophic wind maximum at the base of the geopotential height trough towards an inflection axis in the height field. Wave ducting characterized by a sufficiently deep low-level stable layer on the cold side of the surface front overlaid by a conditionally unstable layer with an embedded critical level appears to be the main wave maintenance mechanism according to most of the observational and numerical studies (Jones, 1968; Lindzen and Tung, 1976; Uccellini and Koch, 1987; Crook, 1988; Koch et al, 1998; Powers and Reed, 1993; Ralph et al, 1993a, b; Monserrat and Thorpe, 1996; Koch et al, 1998; Wang and Lin, 1999; Shen and Lin, 1999). A few studies also have suggested that wave-CISK (Lindzen, 1974; Raymond, 1975; 1984; Powers and Reed, 1993; Powers, 1997; Koch et al, 1998) and solitary wave dynamics (Lin and Goff, 1988) may also maintain the longevity of the gravity waves.

Until recently, many previous gravity wave studies have relied exclusively upon observational analyses. The earliest studies of mesoscale gravity waves using numerical weather prediction models were first conducted by Zhang and Fritsch (1988) and Schmidt and Cotton (1990). Gravity waves in these studies were generated by the simulated mesoscale convective systems. However, detailed verification of these waves against mesoscale observations was not performed due to the unavailability of the mesoscale data sets. The first published attempt to use a mesoscale model for the sole purpose of attempting to simulate and study an observed gravity wave event, and for which verification was performed against detailed mesoanalysis, was provided by Powers and Reed (1993). Since then, mesoscale numerical models have been developed into powerful tools for the detailed study of gravity wave structure, energy sources, and maintenance mechanisms, all of which are difficult to detect with standard observations (Powers, 1997; Pokrandt et al, 1997; Kaplan et al, 1997; Zhang and Koch, 2000; Koch et al, 2001).

An extraordinary large-amplitude mesoscale gravity wave event associated with extratropical cyclogenesis on 4 January 1994 along the East Coast of the United States was recently documented by Bosart et al (1998) (hereafter referred to as B98) with conventional data. The incentive for mesoscale numerical model simulation of this gravity wave event is that, while the National Centers for Environmental Prediction (NCEP) operational prediction models [Regional Analysis and Forecast Systems (RAFS) and Eta] and human forecasters performed admirably in identifying the large scale circulation features associated with storm development, they were much less successful in distinguishing three important embedded mesoscale features in this event. These features were a long-lived, large-amplitude gravity wave, a weak predecessor wave cyclone along a coastal warm front well downstream of the primary surface cyclone, and a heavy snow band that moved northeastward along the Appalachian Mountains. Also, high-resolution information in both time and space is required to study details of gravity wave structure and dynamics. Because the wave generation mechanisms hypothesized by B98 need to be verified and this extraordinary gravity wave event was analyzed purely with conventional observations (not from a mesoscale field experiment), numerical simulations are essential to the study of this event. The climatological study by Koppel et al (2000) suggests that these events occur fairly frequently, yet numerical studies of gravity waves along the East Coast of the U. S. are non-existent in the literature.

In Sect. 2, the gravity wave observations by B98 will be briefly reviewed. The model and experiments will be presented in Sect. 3. Section 4 will compare the control simulation with observations. Sensitivity tests with respect to topography, diabatic heating and grid resolution are given in Sect. 5. Conclusions will be in Sect. 6. Unbalanced flow diagnostics, wavelet and energy transport analysis and the governing dynamics are presented in Zhang (2000), and Zhang et al (2001).

## **2. Review of the observational analysis by Bosart et al (1998)**

Remarkably, the highly detailed case study by B98 did not use data from a field experiment.

Instead, they used conventional surface and upper-air observations, operational WSR-88D Doppler radar and wind profiler observations, satellite imagery, digitized microbarograms, and a few observations from independent observers at stations along the Atlantic coast. Also, the 80-km grid Eta model initialized and forecast fields were used to diagnose the synoptic forcing associated with this gravity wave event, even though the model was incapable of resolving adequately the waves.

Between 00 and 06 UTC on 4 January 1994 multiple small-amplitude gravity waves with northwest-southeast orientation were observed in association with an ordinary extratropical cyclone moving northward along the Atlantic coast. The incipient gravity waves rapidly amplified around 0600 UTC over a region of cold air damming upstream of a high, cold cloud shield located on the northern edge of a warm front. The dominant gravity wave was first detectable as a consistent feature across northeastern North Carolina and Virginia at 0700 UTC, which amplifies and accelerates northeastward. The dominant wave was a wave of depression during the first several hours but it developed into a series of waves after 1200 UTC as it propagated toward New England. The observed phase speed was higher ( $30\text{--}40\text{ m s}^{-1}$ ) in New England than that over the mid-Atlantic states ( $\sim 25\text{ m s}^{-1}$ ). The wavelength was 100–200 km across New England with a peak crest-to-trough pressure fall  $>10\text{ hpa}$  in 20–30 minutes. Short-lived blizzard conditions such as heavy snow and ice pellets were associated with the passage of the wave crest. Peak surface wind occurred just prior to the wave-induced minimum in the mean sea-level pressure. However, many of these conclusions were tentative because of the lack of sufficiently detailed observations and model forecast fields.

The analyses by B98 also showed that this gravity wave event conformed with the Uccellini and Koch (1987) conceptual model, since the gravity waves occurred in a divergent region bounded by the 300-hpa geopotential ridge axis to the northeast, the 300-hpa inflection axis to the southwest, and a surface frontal boundary to the southeast. B98 suggested three possible gravity wave *genesis* mechanisms: (1) shear instability, (2) unbalanced flow and associated geostrophic

adjustment, and (3) mechanical perturbation of the wave duct by strong vertical motions. They further hypothesized the following possible gravity wave *amplification* mechanisms: (1) over-reflection in the increasingly strong wave duct; and (2) positive feedback between ascent, latent heat release, and wave growth due to vigorous perturbation of the inversion by vertical motions associated with wave-induced latent heat release. Wave ducting (Lindzen and Tung, 1976) was proposed to be the primary *maintenance* mechanism for the dominant large-amplitude gravity wave. They also pointed out the possible wave origin in the upper troposphere and the attendant downward energy transport. The major goals of the current study are: (1) to test the ability of a high-resolution mesoscale model in simulating the exceptionally large-amplitude gravity wave event documented by observational analysis and (2) to perform various sensitivity tests to validate the simulated gravity waves and to isolate the generation mechanisms of the gravity waves. The governing dynamics of the gravity wave generation and maintenance and the comparison with the various conjectures of B98 was explored in great detail in Zhang et al (2001).

### 3. Model and experiments

The numerical model used is the nonhydrostatic, primitive equation NCAR-Pennsylvania State University Mesoscale Model 5 Version 2 (MM5V2) (Dudhia, 1994; Grell et al, 1995) run on two grid meshes with horizontal resolutions of 36 km and 12 km. Both domains are shown in Fig. 1. The experiments performed for this study are listed in Table 1. For the control run, the coarse domain (domain 1) was initialized at 0000 UTC 4 January 1994 with NCEP global grid analysis as the first guess and was reanalyzed with surface and upper-air observations. The 12-km nested domain (domain 2) was initialized at 0300 UTC from the coarse domain. The Kuo-Anthes and Grell convective parameterization schemes (Kuo, 1974; Anthes, 1977; Grell, 1993) were used for the coarse and nested domains, respectively; both domains employed Reisner 2 explicit microphysics scheme (Reisner et al, 1998). The Blackadar planetary boundary-layer scheme (Zhang and Anthes, 1982) and the upper radiative boundary condition (Klemp and

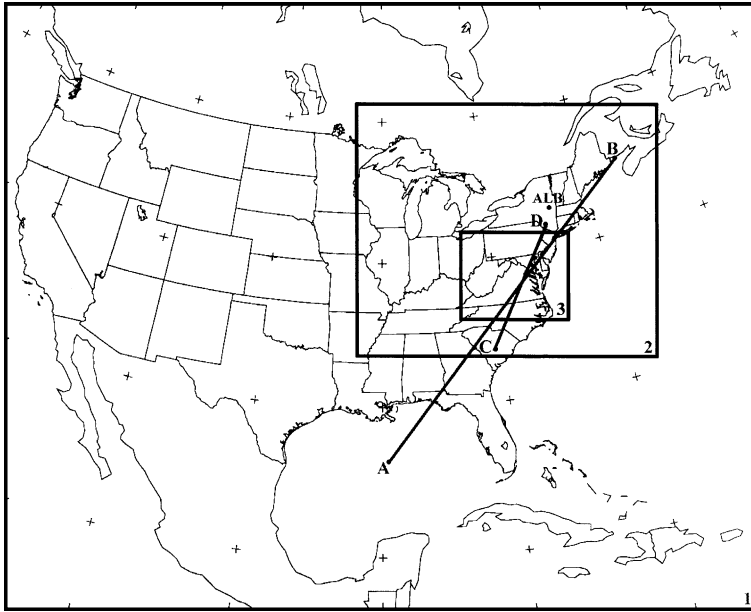


**Fig. 1.** Model domains for the MM5 simulations. The grid resolutions for Domain 1, 2, and 3 are 36, 12, and 4-km, respectively. Line A–B indicates the location of the cross section for domain 1. Line C–D indicates the location of the cross section for domain 2. Albany (ALB), New York is shown as ALB

**Table 1.** Summary of MM5 experiments. Resolutions of the coarse and nested fine grids are shown separately by slash (/), i.e., 36/12 refers to 36 km coarse/12 km fine grid; likewise initialization (“start”) times of the two grids are shown separately by slashes

Experiment	Grid (km)	Start time	Moisture schemes	Purposes of experiment
Control Run	36/12	00/03 UTC	Explicit + Kuo-Anthes/Grell	Full physics, control run
No-Appalachians	36/12	00/03 UTC	Explicit + Kuo-Anthes/Grell	Topography effect, examined by reducing the Appalachians heights by 90%
Fake-Dry-A	36/12	00/03 UTC	Explicit	Latent heating/cooling effect, fake-dry from 00Z
Fake-Dry-B	36/12	00/03 UTC	Explicit	Latent heating/cooling effect, fake-dry from 06Z
Fake-Dry-C	36/12	00/03 UTC	Explicit	Latent heating/cooling effect, fake-dry from 08Z
4 km-Run	4	05 UTC	Explicit	Sensitivity to grid resolution, initiated from the control run
Early-Run	36/12	12Z 3 Jan	Grell/Grell	Sensitivity to initialization, and one-way or two-way nesting

Durrán, 1983) were used. Observational analyses provided the lateral boundary condition for the coarse domain, and the coarse domain provided one-way boundary conditions for the nested domain. Both domains invoked a flow relaxation scheme for their lateral boundary conditions (Duhdia, 1994). The model was run for 24 hours without pre-forecast nudging or any other special initialization procedure.

Several “Fake-Dry” simulations (thermodynamic effects of phase change of water substance disallowed) and a “No-Appalachians” simulation

were performed, respectively to explore the role of diabatic heating and topography in the gravity wave generation, amplification and maintenance. In simulation “Fake-Dry-A”, the latent heating/cooling was turned off from the very beginning of the simulation. In “Fake-Dry-B” and “Fake-Dry-C”, both experiments were performed exactly the same as the control run except that the latent heating/cooling was cut off 1 hour before (from 0600 UTC) and 1 hour after (from 0800 UTC) the first appearance of the dominant surface gravity wave, respectively. In simulation

“No-Appalachians”, the terrain heights of the Appalachian Mountains were “reduced” to one tenth of their original value while the terrain elsewhere (including the Rockies) was kept unchanged.

The “4 km-Run” was a 4-km grid simulation (domain 3) initialized at 0500 UTC from the fine grid of the control simulation and with no cumulus parameterization for domain 3 (only fully explicit microphysics). This experiment was performed to study the sensitivity of the gravity wave forecast to the model grid resolution and the uncertainties owing to the choice of cumulus parameterization scheme compared to explicitly-resolved moist convection. The relative location of this ultra-fine domain is also shown in Fig. 1.

The “Early-Run” experiment was initialized at 1200 UTC 3 January 1994 for both Domain 1 and Domain 2, 12 hours earlier than the control run and ~20 hours prior to the observed large-amplitude gravity wave generation. Both model domains used the Grell cumulus parameterization scheme and with two-way nesting capability. This experiment was performed to study the sensitivity of the gravity wave simulation to model initialization.

#### 4. Control simulation

The MM5 control run forecasts (Fig. 2) compare well with the synoptic-scale observational analysis of B98 and replicate such Eta model

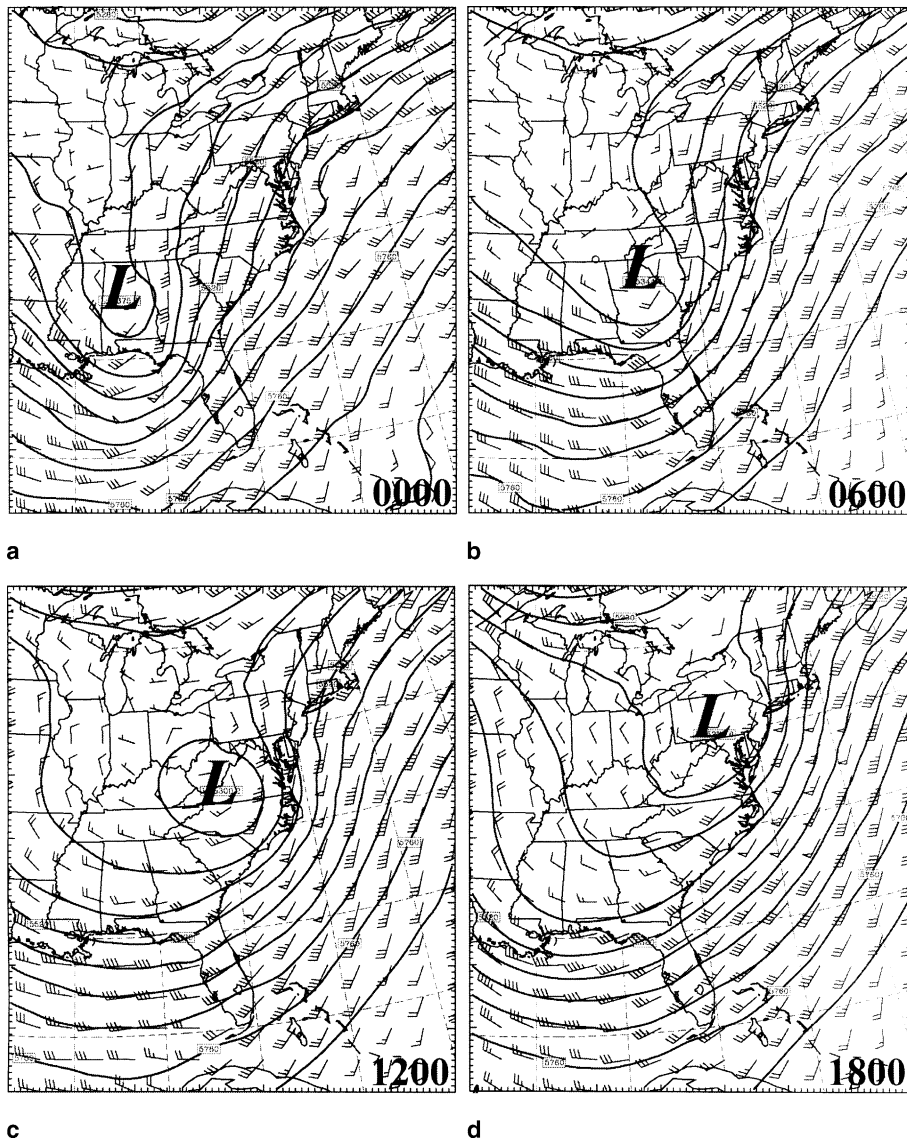


**Fig. 2.** Coarse grid simulated 500-hpa geopotential heights (solid, every 6 dam) and wind vectors (full barb denotes  $10 \text{ m s}^{-1}$ ) for **a** 0000, **b** 0600, **c** 1200, and **d** 1800 UTC 4 January 1994

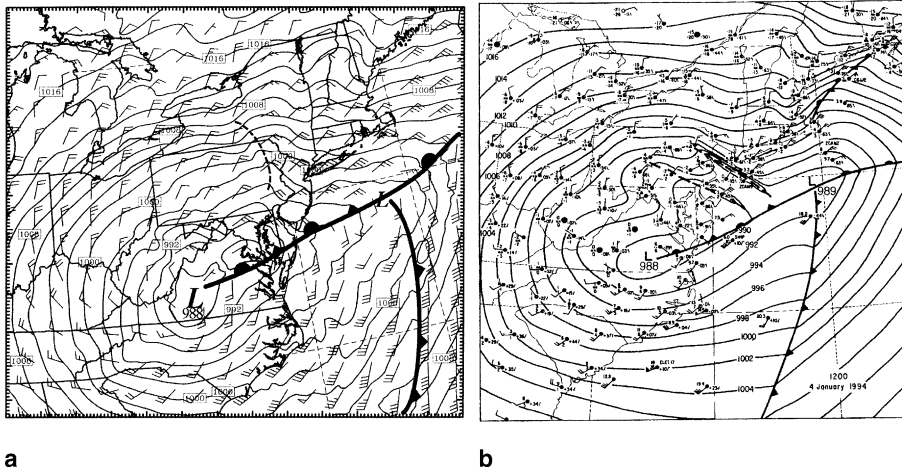


**Fig. 3a.** Fine grid forecast sea level pressure (every 2 hPa) and surface winds (full barb  $5 \text{ m s}^{-1}$ ) for 1200 UTC 4 January 1994; **b** Subjective surface observational analysis (from Bosart et al, 1998). The dashed lines depict gravity wave troughs

features as the jet core strength and location and the cyclone center (see their fig. 3). At 0000 UTC, the 500 hPa jet streak is over the northeast part of the Gulf of Mexico entering western Florida and the upper-level low is over Alabama (Fig. 2a). By 0600 UTC, the 500 hPa cyclone center has shown slow movement eastwards, the jet core has moved off the coast of the southeastern United States, and the deep trough has become negatively tilted (Fig. 2b). At 1200 UTC, the surface low-pressure center has become positioned over southwest Virginia and the jet core has progressed farther north off the Atlantic Coast (Fig. 2c). This northeastward propagation continues through 1800 UTC, at which time the jet streak is approaching the coast of New England (Fig. 2d).

The 12-h surface forecast valid at 1200 UTC also is in excellent agreement with the observations with respect to strength and location of the cyclone and the frontal features (Fig. 3). In both

the model and observations, the low surface pressure center located in extreme southern Virginia is 988 hPa; the cold front has been pushed far off the Atlantic Coast and an occluded front extends from the cyclone center east-northeast to a triple point east of New Jersey. Strong gravity wave activity in both the model and the observations appears over Pennsylvania and New York, though there is only one wave of depression in the model versus two in the observations at this time.

The 6-hour accumulated precipitation from 0600 to 1200 UTC forecast by MM5 and analyzed by B98 are compared in Fig. 4. The model was very successful in forecasting the intensity, timing and location of the heavy snow band (“snow bomb”) along the Appalachian Mountains. This feature was missed by the operational forecast models (B98). Also, the pronounced precipitation band offshore corresponds well with the strong convective band seen in the same

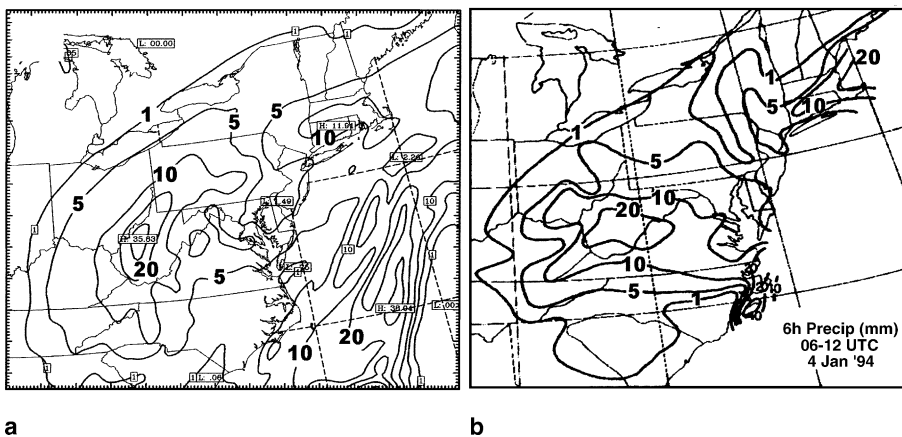


**Fig. 4a.** Fine grid simulated accumulated precipitation (solid, contoured every 1, 5, 10, and 20 mm) from 0600 to 1200 UTC 4 January 1994; **b** As in panel a, except for the observational analysis (from Bosart et al, 1998)

location in infrared satellite imagery (see fig. 12 in B98) although the precipitation was significantly underestimated over extreme eastern North Carolina. This successful precipitation forecast suggests that the moist processes (including convection) were handled well by the control simulation.

All the comparisons above showed that the control simulation was successful in providing an accurate 24-hour large-scale forecast. Moreover, MM5 simulated reasonably well the observed dominant large-amplitude gravity wave. Isochrones of the fine grid simulated dominant gravity wave as analyzed from the mean sea-level pressure field are compared to those from the observational analysis by B98 in Fig. 5. The forecast gravity wave at the surface was first detectable at 0700 UTC in eastern Virginia with a horizontal wavelength  $\sim 100$  km. This wave propagated up the East Coast as far as eastern New York with a speed of  $22.5 \text{ m s}^{-1}$ . The timing, wavelength and the phase speed are all quite similar to those observed, though the “wave corridor” was  $\sim 100$ – $200$  km too far inland, and the wave-fronts display a somewhat different orientation and shape.

While it was not possible to identify the individual gravity waves in the sea-level pressure field before 0600 UTC, there were clear gravity wave signals in the middle troposphere as early as 0330 UTC over South Carolina. Therefore, the actual gravity wave generation region was upstream of that depicted in Fig. 5. Evidence for this claim can be found in the time-distance

cross section analyses used to study the height variation of the wave characteristics (Fig. 6). The time evolution of the vertical motion fields at the selected sigma levels (which are approximately 812, 714, 615, 516, 417 and 295 hpa levels) was plotted at 15-minute intervals. Analyses using direct sigma level data should be sufficient for the specific cross section chosen because the underlying terrain is nearly flat (Fig. 1). This analysis reveals that while the dominant gravity wave B2 began to take on a discernable structure at all levels after 0600 UTC, it evolved from a broader upward motion band (incipient wave B) as far back as 0315 UTC. This upward motion band and a companion downward motion band were persistent in the layer from 750 to 600 hpa (Fig. 6b, c).

From 0600 to 0700 UTC, the vertical motion fields in Fig. 6 exhibited rapid amplification and scale shortening. During this time, convection associated with this upward motion band developed (fig. 6 of Zhang et al, 2001) and the gravity wave became evident at the surface. However, the analyses in Fig. 6 and also in Zhang et al (2001) show no evidence of convective activity associated with this incipient wave (or updraft band) before 0630 UTC.

Figures 7 and 8 show “zoomed-in” depictions of the dominant gravity wave at the surface and in vertical cross section format, respectively. The peak to trough double amplitude of the surface gravity wave at 1000 UTC was  $\sim 3$ – $4$  hpa and the horizontal wavelength was  $\sim 100$  km with the distance between the pressure trough and

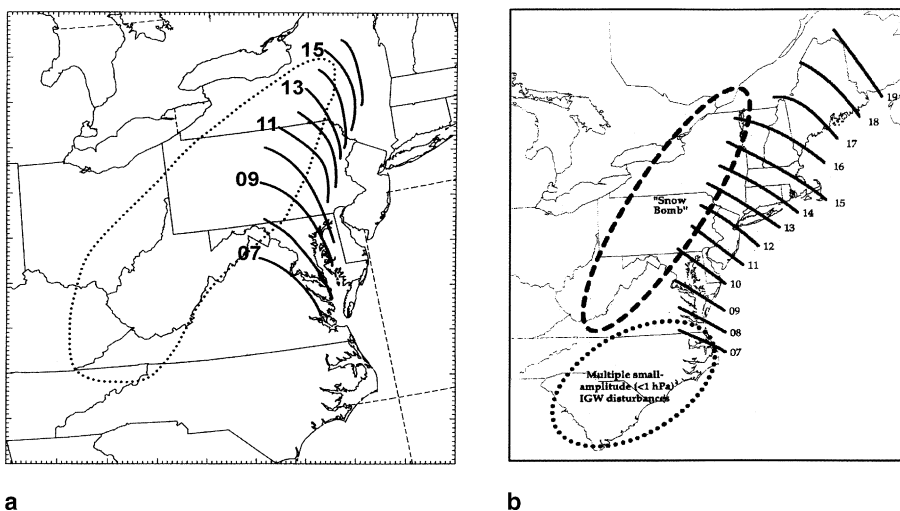


**Fig. 5a.** Isochrone analysis of fine grid simulated gravity wave for 4 January 1994. Area with accumulated precipitation from 00 to 18 UTC greater than 20 mm is outlined by dotted line; **b** Observational analysis (from Bosart et al, 1998)

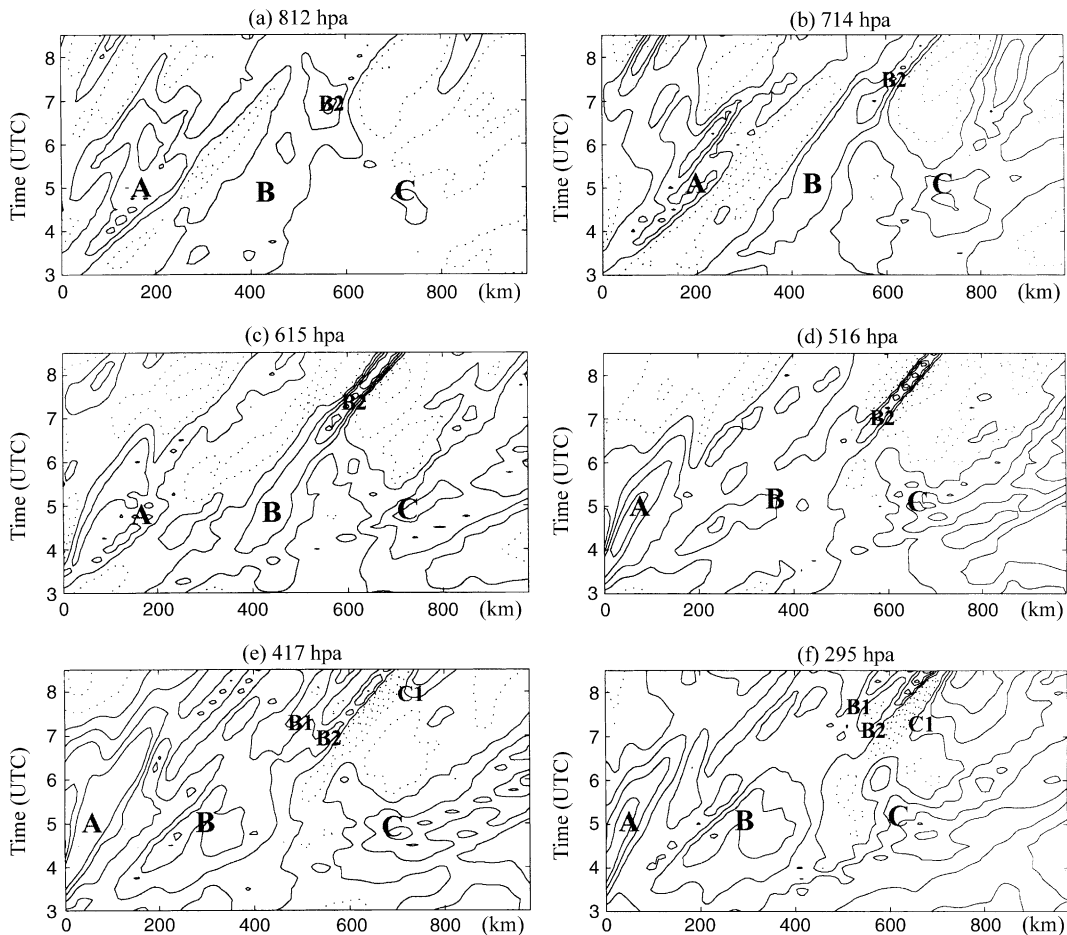


**Fig. 6.** Fine grid time-space evolution (“ray tracing”) of the vertical motion ( $\Delta = 5 \text{ ms}^{-1}$ , solid line, positive, and dashed line, negative) along the cross section (see line C–D in Fig. 1) for **a** 812, **b** 714, **c** 615, **d** 516, **e** 417, and **f** 295 hpa from 0300 to 0830 UTC 4 January 1994. Labels “A”, “B”, and “C” indicate the locations of the 200-km scale waves and “B1”, “B2”, and “C1” represent the locations of the 100-km scale waves as revealed by the wavelet analyses in Zhang et al (2001)

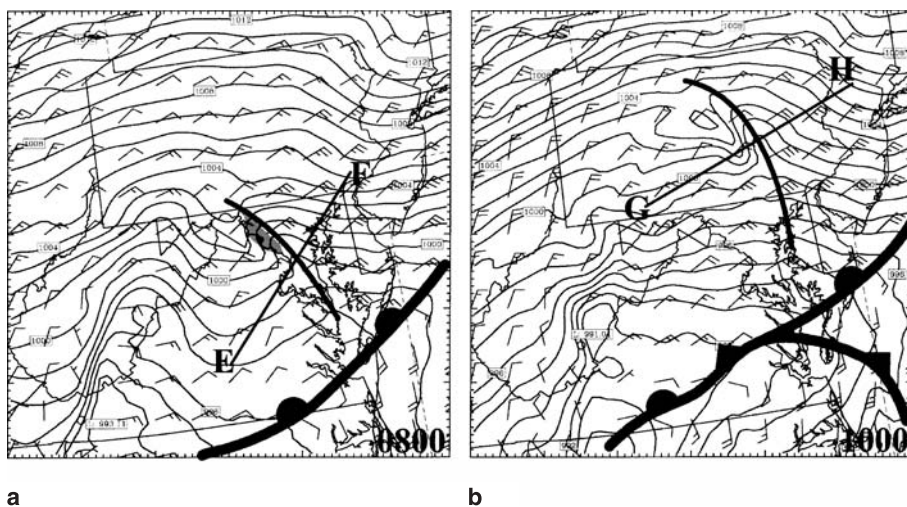


**Fig. 7.** As in Fig. 3a, but for **a** 0800, and **b** 1000 UTC 4 January 1994 and using 1 hpa intervals. Lines EF and GH indicate the cross sections in Figs. 8a and b, respectively. The 850 hPa upward motion associated with the dominant gravity wave greater than  $15 \text{ cm/s}$  is shaded in **a**

the upstream ridge slightly longer than the distance between the pressure trough and the downstream ridge. During the early stage of the

gravity wave (e.g., 0700 UTC, Fig. 8a), the wave showed an upstream tilt with a pronounced phase shift existing just above or at the critical level

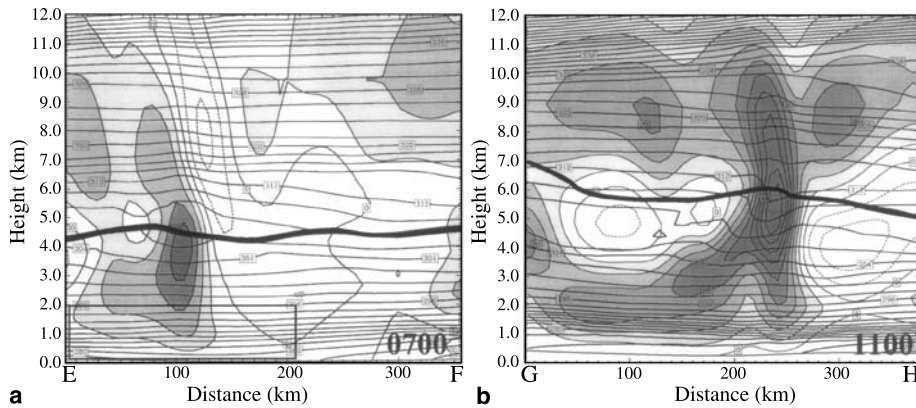


**Fig. 8.** Fine grid vertical cross sections (lines EF and GH in Fig. 7, respectively) of forecast potential temperature (solid lines,  $\Delta = 2$  K), vertical velocity ( $\Delta = 5$  cm s<sup>-1</sup> with shaded area  $w > 5$  cm s<sup>-1</sup>) and critical level (thick solid lines) from the control circulation at **a** 0700, and **b** 1100 UTC 4 January 1994. The rectangular box on the left bottom of panel **a** indicates the relative location of Fig. 11

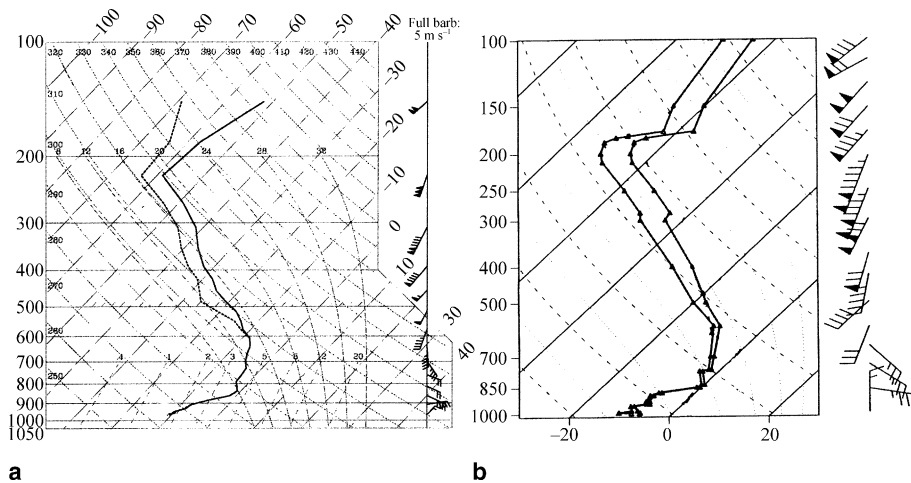


**Fig. 9.** Sounding in skew T-log format for Albany (ALB), New York for 1200 UTC 4 January 1994; **a** MM5 domain 2 12-h forecast, **b** observation (after Bosart et al, 1998). The winds are plotted with one pennant, full barb, and half-barb denoting 25, 5, and 2.5 m/s, respectively

( $Z_c$ ). There is no apparent tilt below the critical level. However, by 1100 UTC, more of a wave-CISK shape developed with much less evidence of tilt and the maximum upward motion was further lifted to  $\sim 5.5$  km (Fig. 8b). The strong updraft collocated with an apparent warm temperature anomaly, both maximized near the critical level, implies that the convection was moving along at the same speed as the gravity wave (Lin, 1987). These structural and phase relationships are consistent with a wave-CISK model by Raymond (1984), according to which organized convection is forced by convergence associated with a gravity wave, while latent heating within the convection provides a source of wave energy.

The model forecast sounding valid at 1200 UTC for Albany (ALB), New York, which is located in the area where the gravity wave was

the strongest, may be compared with that observed in Fig. 9. The model simulated the observed inversion layer beneath 850 hPa and a thick near-saturated layer above it up to  $\sim 620$  hPa. The jet maximum at 250 hPa and the strong shear layer beneath it are also well simulated though 500–400 hPa layer winds are slightly stronger than observed.

Synthesis of Figs. 2b, 5, and 7a shows that the dominant large-amplitude gravity wave in both the MM5 simulation and the observations formed in a region bounded by the 300-hPa ridge to the northeast, the trough axis to the southwest, and a surface warm front boundary to the southeast as the jet streak approached the 300 hPa inflection axis. This kind of large-scale environment is consistent with the Uccellini and Koch (1987) conceptual model for mesoscale gravity waves, according to which geostrophic adjustment and

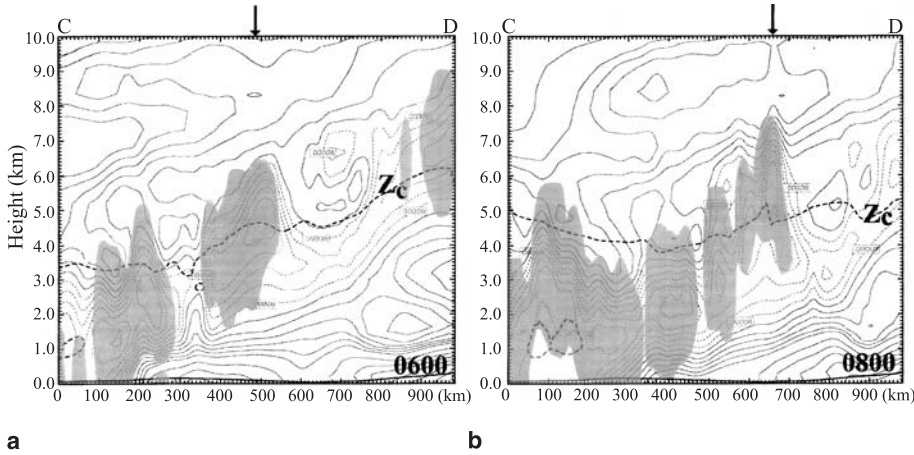


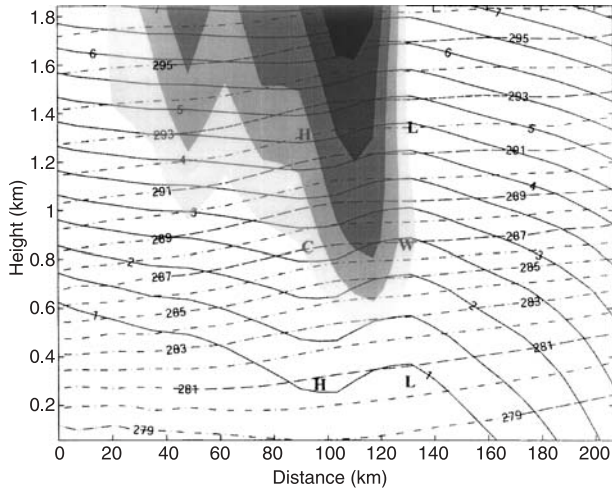
**Fig. 10.** Fine grid cross section (line C–D in Fig. 1) of square of moist Brunt-Vaisala frequency ( $N^2$ ,  $\Delta = 0.00002 \text{ s}^{-2}$  for  $N^2 < 0.002 \text{ s}^{-2}$  and  $\Delta = 0.00004 \text{ s}^{-2}$  for  $N^2 > 0.002 \text{ s}^{-2}$ ; thin dashed lines indicate  $N^2 < 0.0008 \text{ s}^{-2}$ ) for **a** 0600, **b** 0800 UTC 4 January 1994. The area shaded indicates Richardson number  $Ri < 0.25$  and the thick dashed lines shows the wave critical level, assuming a wave speed of  $22.5 \text{ m s}^{-1}$ . The arrow indicates the location of the dominant gravity wave. The thick dashed lines marked by  $Z_c$  denotes the location of the critical levels

shear instability are the most likely mechanisms to initiate the gravity waves. Nevertheless, the exact process by which the flow becomes unbalanced, gravity-inertia waves are generated, and the wave energy at or near the jet level penetrates downward to perturb the duct layer has never been satisfactorily explained.

Wave ducting of mesoscale gravity waves proposed by Lindzen and Tung (1976) was also examined. The cold air beneath the warm front built up a 1.5–2.5 km thick stable layer with mean Vaisalla-Brunt frequency  $N = 0.012 \text{ s}^{-1}$  immediately downstream of the dominant gravity wave. This duct layer is overlain by a layer containing small static stability extending to 3–6 km (Fig. 10). A single critical level (thick dashed line) exists in the less stable layer and the Richardson number  $Ri < 0.25$  in a shallow region surrounding the critical level (Fig. 10). The intrinsic ducted wave speed is given as  $C_{d,n} = \frac{ND}{(\pi/2+n)}$ , where  $n$  indicates different vertical wave modes and  $N$  includes the liquid water effect. For the primary mode ( $n = 0$ ), and a duct layer of depth  $D = 2.0 \text{ km}$ , the predicted ducted wave speed  $C_d \sim 20.0 \text{ m s}^{-1}$ . With a mean wind speed of  $5 \text{ m s}^{-1}$  in this layer, the ground relative ducted wave speed is  $25.0 \text{ m s}^{-1}$ , which compares well to the average simulated phase speed of  $22.5 \text{ m s}^{-1}$ . Because of the strong variation of stratification and shear properties throughout the

troposphere, the vertical wavelength of the gravity wave could vary with height and may not be easily estimated. This environment provides an excellent wave duct if the vertical wavelength of the gravity wave is roughly 4 times of the stable layer depth or  $\sim 8.0 \text{ km}$  (Lindzen and Tung, 1976). It should also be noted that, because of the strong temporal and spatial variability of the environment (note the differences occurring in only 2 hours between Fig. 10a and b), the ducting analysis estimated from individual soundings (as used by B98) may not be representative. Also, the duct property may also be modified by the gravity wave itself. Accordingly, the above ducting analysis only represents the averaged property of the wave duct.

It is worth mentioning that the simulated pressure perturbation (disturbance “B”) does have the characteristics of an internal gravity wave. The wave-induced pressure and potential temperature perturbations and vertical motions in the ducted layer (Fig. 11) exhibit the essential dynamics of a gravity wave and are consistent with the conceptual gravity wave model of Eom (1975): the cold (warm) anomaly was collocated with the high (low)-pressure perturbation and the maximum upward motion was 1/4 of the horizontal wavelength ahead of the high (cold) anomaly (in other words, ascent produces cooling with the coldest temperatures 1/4 horizontal



same location with similar intensity (not shown). The results from this sensitivity test suggested that, though the Appalachian Mountains are an essential element for cold air damming, they were not critical to gravity wave generation and the heavy precipitation band. In other words, the gravity waves were not forced either by the mechanical perturbation of the upper-level jet streak by topography (Kaplan et al, 1997) or a gravity current or bore generated by topography (Karyampudi et al, 1995a, b; Zhang and Koch, 2000; Koch et al, 2001), or any other topographic mechanism suggested in recent modeling studies of gravity waves. Note that the model was initialized at 0000 UTC when the cold air damming was already present. Therefore, cold air was already in place for providing a favorable duct for the gravity waves even in this “No-Appalachians” simulation with similar properties to that of the control simulation (not shown).

### 5.2 “Fake-Dry-A”

Several “fake dry” simulations with the latent heating/cooling associated with the phase change of water substance turned off at different stages of the gravity wave development were also performed (Table 1). In the simulation where the diabatic heating was cut off from the very beginning of the run (“Fake-Dry-A”), the model failed to predict large-amplitude gravity waves. However, it is very important that there were signals of the incipient wave (“B”) prior to ~0600 UTC in the middle troposphere as shown in Fig. 13. Wave “B” from “Fake-Dry-A” is very similar to the incipient gravity wave (“B”) found in the control simulation (Fig. 6) prior to ~0600 UTC.

By turning off the latent heating from the very beginning of the model simulation, the extratropical cyclone was much weaker than that in

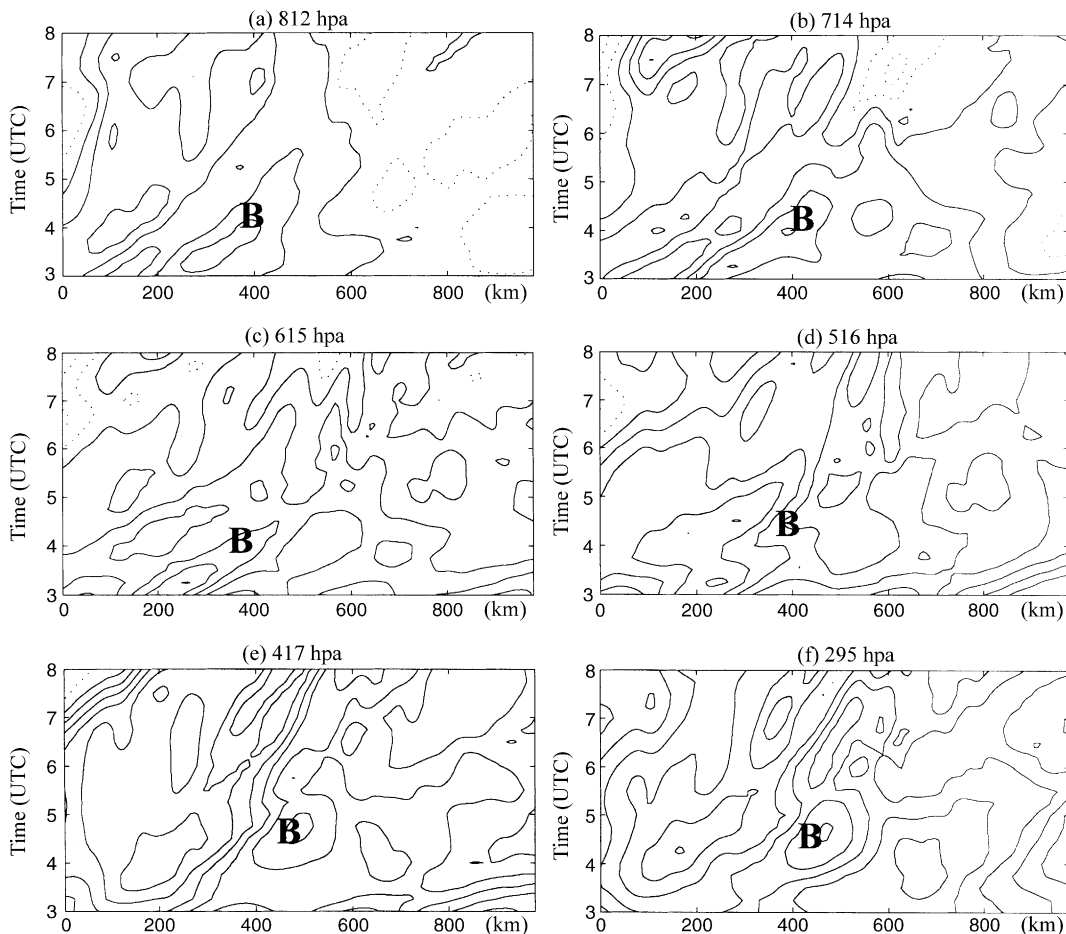


**Fig. 13.** Simulation “Fake-Dry-A” time-space evolution of the vertical motion ( $\Delta = 3 \text{ m s}^{-1}$ , solid line, positive, and dashed line, negative) along the cross section (see line C–D in Fig. 1) for **a** 812, **b** 714, **c** 615, **d** 516, **e** 417, and **f** 295 hpa from 0300 to 0800 UTC 4 January 1994

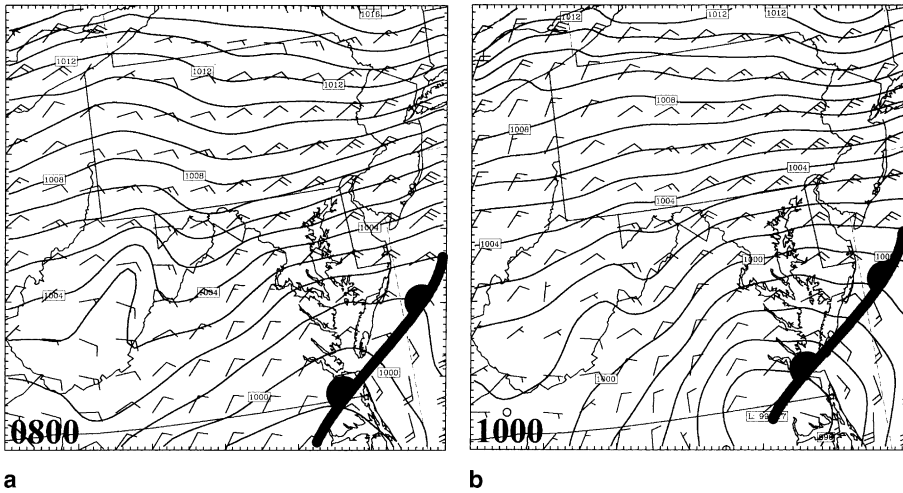


**Fig. 14.** As in Fig. 3a, but for simulation “Fake-Dry-A” at **a** 0800, and **b** 1000 UTC 4 January 1994

the control simulation. By 1200 UTC, the surface low-pressure center (994 hpa) was 6 hpa weaker than that in the control run and the observations (988 hpa). Because the large-scale environment and unbalanced dynamics have been changed in this “Fake-Dry-A” simulation (Fig. 15 of Zhang et al, 2001) before the actual gravity wave generated, the results from this sensitivity test are too ambiguous to use for assessing the relative roles of geostrophic adjustment and convection in the gravity wave genesis. The effectiveness of using “Fake-Dry” simulations such as those conducted by Powers and Reed (1993), was also questioned by Pokrandt et al (1997). The fact that there were still incipient gravity waves in this simulation, even though they were not seen at the surface (Fig. 14), suggests that the convective activity modifies the balanced dynamics of the large-scale baroclinic wave, which in turn affects the gravity wave generation through geostrophic adjustment. This conjecture, as well as the role of

localized convective heating in the rapid amplification of the gravity waves, are both examined in great detail in Zhang et al (2001).

5.3 “Fake-Dry-B”

In simulation “Fake-Dry-B”, the latent heating/cooling was cut off at 0600 UTC, approximately 1 hour before the large-amplitude gravity wave first appeared at the surface maps in the control run. The incipient gravity waves in the middle-troposphere still persisted for a short period of time. However, they never amplified but instead weakened rapidly. As in the “Fake-Dry-A” simulation, the gravity waves could not be easily discerned in the mean sea level pressure field (Fig. 15a). This result further suggests that convection was playing a key role in transporting the middle-upper tropospheric wave energy downward and also in amplifying the waves.

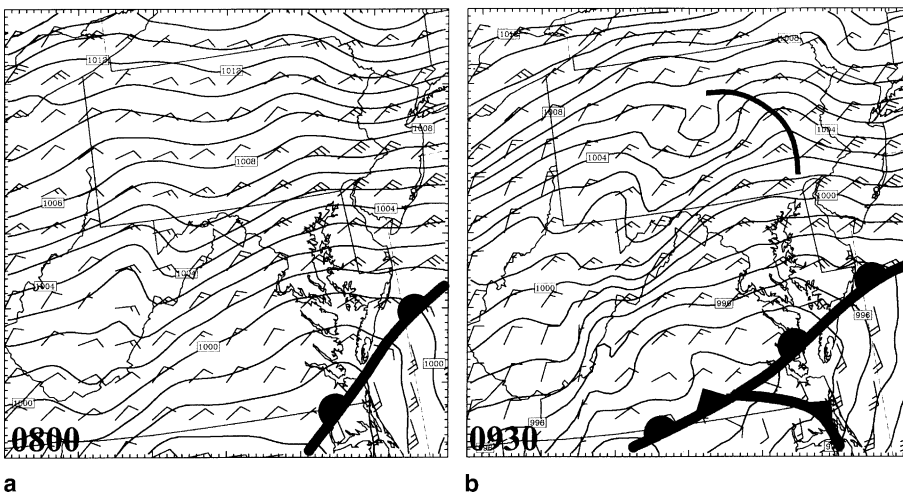


**Fig. 15a.** As in Fig. 3a, but for simulation “Fake-Dry-B” at 0800 UTC 4 January 1994; **b** As in Fig. 3a, but for simulation “Fake-Dry-C” at 0930 UTC 4 January 1994

#### 5.4 “Fake-Dry-C”

The latent heating/cooling in simulation “Fake-Dry-C” was cut off one hour after the first appearance of the gravity wave at the surface in the control run, i.e., at 0800 UTC. The gravity waves were temporarily sustained in this simulation in the mean sea-level pressure fields, but they rapidly weakened over the next few hours (Fig. 15b). In fact, by 1000 UTC, the surface gravity wave had disappeared entirely. Results from this simulation suggest that wave-CISK was essential to maintenance and amplification of the simulated gravity waves, despite the favorable wave ducting environment. Further evidence of enhanced downward energy transport with diabatic heating can be found in fig. 19c of Zhang et al (2001).

#### 5.5 Sensitivity of waves to grid resolution

Because cumulus convection was still parameterized in the 12-km simulation, we also performed an experiment with 4-km horizontal grid resolution where no cumulus parameterization (“4 km-Run”) was used to test the sensitivity of the gravity wave simulation with regard to the grid resolution and convective schemes. The 4-km grid simulation should have marginally resolved convection explicitly. Though an even higher grid resolution simulation is desirable, the large domain of the gravity wave activity and the limited computing resources prevented that from being done. The “4 km-Run” started at 0500 UTC, using the 12-km resolution model forecast at that time as the initial and boundary conditions.

The results from this third “ultra-fine” domain agreed quite well with that of the 12-km fine grid, including gravity waves with similar dominant wavelength and amplitude, though the convection associated with the gravity wave appeared about 15~30 minutes earlier. The “4 km-Run” also resolved gravity waves with much smaller wavelengths and more than a single wave was apparent (Fig. 16), similar in that regard to the observational analysis (Fig. 3b). However, the amplitude of the dominant gravity wave was slightly weaker since more wave energy resided in smaller scales than in the 12-km simulation [see the discussion in Powers (1997)]. Moreover, this simulation confirms that the dominant gravity wave in the control simulation was not an artifact of the cumulus parameterization schemes used.

#### 5.6 Sensitivity to initialization

Because the gravity waves were generated only 4–6 hours after the initialization in the control simulation, it may be questioned whether the gravity waves were generated or modified by an initial disturbance (a mass-momentum imbalance) arising from the use of the static initialization. To assess the evolution of the initial “noise” due to the initialization of the 0000 UTC 4 January control simulation, the domain-average second derivative of surface pressure (which is directly related to the mass divergence tendency through the continuity equation, Manobianco et al, 1994) was computed (Fig. 17). This diagnosis showed that after 2–3 hours of model integration, gravity wave disturbances due to the initialization imbalance had fully

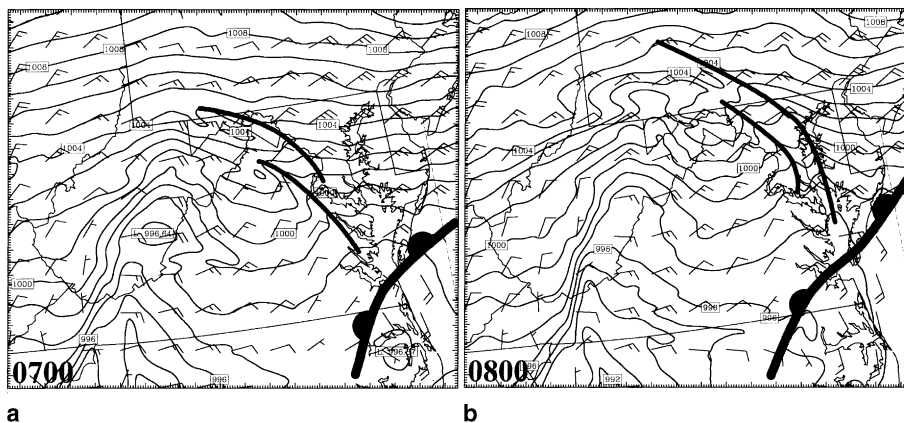


**Fig. 16.** As in Fig. 3a, but for domain 3 of simulation “4 km-Run” at **a** 0700, and **b** 0800 UTC 4 January 1994

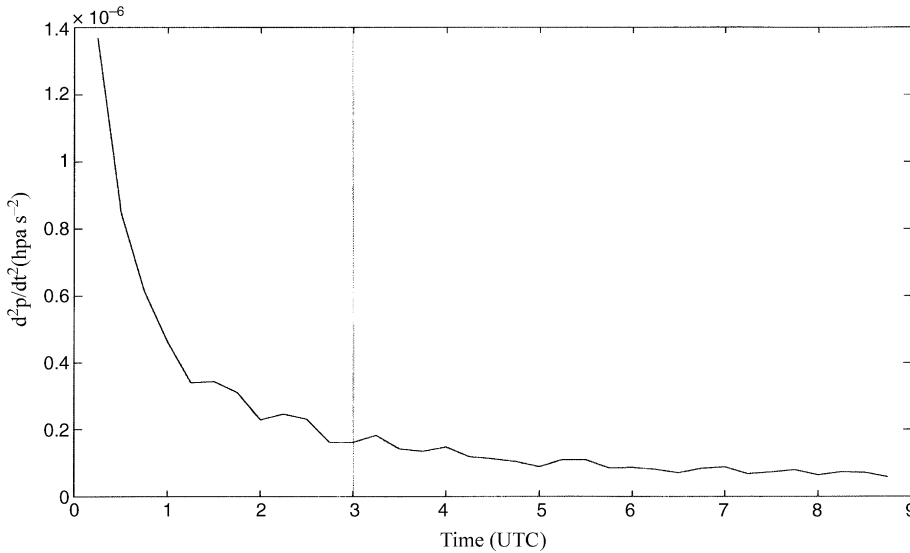


**Fig. 17.** Time series of magnitude of the domain-average second time derivative of surface pressure ( $\text{hpa s}^{-2}$ ) for coarse grid of the control simulation

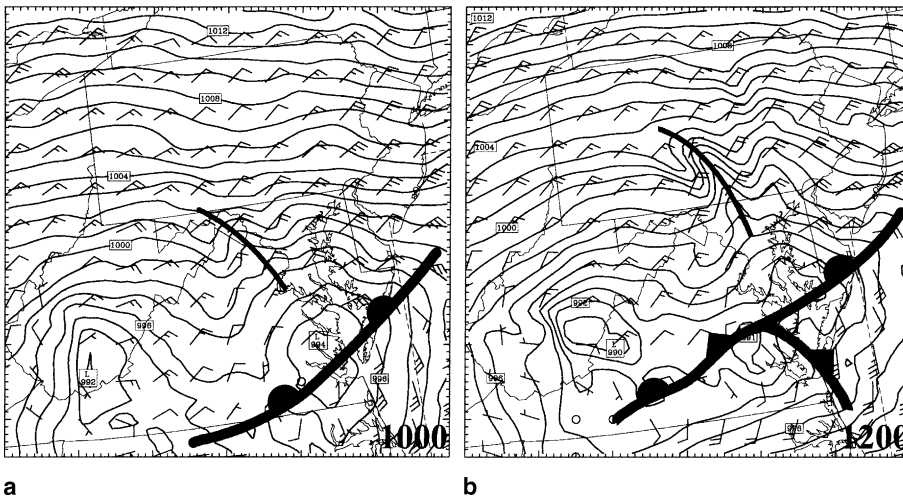


**Fig. 18.** As in Fig. 3a, but for the “Early-Run” at **a** 1000, and **b** 1200 UTC 4 January 1994 and using 1 hpa intervals

subsided. In this respect, results from the control simulation of the dominant gravity wave were reliable.

The sensitivity of the simulated gravity waves to the model initialization is further tested with another experiment “Early-Run”, which is initialized  $\sim 20$  hours prior to the observed gravity wave at the surface. In the “Early-Run” experiment, both domains 1 (36-km grid) and 2 (12-km grid) were initialized at 1200 UTC 3 January 1994 with the two-way nested boundary conditions. The simulated gravity waves in “Early-Run” (Fig. 18) are qualitatively similar to those in the control experiment except for a two-hour timing difference between these two experiments. The “Early-Run” sensitivity experiment confirms that the simulated gravity wave is not

an artifact of the one-way nested boundary conditions or the false imbalance from the initial conditions.

## 6. Conclusions

Numerical simulations have been performed so as to study the scale-interactive dynamics of a large-amplitude gravity wave event on 4 January 1994 along the East Coast of the United States recently documented by B98. One-way nested MM5 simulations have been performed with horizontal grid sizes of 36, 12 and 4 km. Results from the MM5 control simulation compared well with the synoptic scale observational analysis with respect to the jet and cyclone evolution. Moreover, the model showed strong skill in

forecasting three prominent mesoscale features, i.e., the dominant large-amplitude gravity wave, snow band, and precursor warm wave front embedded within the cyclone, which were not well-forecasted by the real-time models. The simulated gravity wave was generated with timing, location, wavelength and propagation speed similar to those observed by B98. Analyses showed that the large amplitude gravity wave was generated in a synoptic-scale environment comparable to the Uccellini and Koch (1987) conceptual gravity wave model. Thus, the wave formed where the jet streak encountered unbalanced conditions at an inflection point in the upper-level geopotential field downstream of the trough and to the cool side of the surface warm front. However, in addition, there were strong upstream frontal circulations (warm occlusion and tropopause folding) prior to and during the gravity wave generation. Model simulation fields and observations both showed that ducting criteria were nearly satisfied along the path of the gravity waves.

Several sensitivity tests were performed. Results from these simulations suggested that topography was not directly responsible for gravity wave genesis, but that latent heating was necessary to amplify and maintain the large-amplitude gravity wave. Gravity wave activity was present though quite weak in the simulation without any latent heat release from the very beginning of the forecast and the dominant observed gravity wave was never realized at the surface. The upper-level jet and cyclone intensity were reduced in this simulation. A slightly stronger gravity wave occurred when the heating was turned off one hour before the surface wave developed. In the simulation with the heating turned off one hour after the surface gravity wave was generated, the dominant gravity wave was sustained for the next few hours with similar characteristics, though it reduced rapidly. Although diabatic heating thus appeared to play an important role in gravity wave amplification and maintenance, convection played no direct role in the wave generation process as shown in Zhang et al (2001).

A 36-km grid resolution simulation barely resolved the 100-km wavelength gravity waves. The 4-km resolution simulation also confirmed that the simulated gravity waves were not an

artifact of the particular (Grell) cumulus parameterization scheme used in the control simulation.

All these aforementioned simulations and analyses have been used to study the governing dynamics of the gravity waves in Zhang et al (2001). It was shown therein that unbalanced flow associated with geostrophic adjustment created a favorable environment near the tropopause fold for gravity wave generation while the merger of the incipient gravity wave with a mid-tropospheric split front directly forced the large-amplitude gravity wave. It was also discussed how the incipient gravity waves with wavelengths longer than 200 km were modified by the feedback from moist convection that developed immediately thereafter along the wave front. Subsequently, ducted wave-CISK modes quickly developed in the model. This kind of gravity wave appears most frequently in mesoscale model simulations (Koch et al, 1999). Whether this occurs in nature with such regularity needs to be verified with direct observations from wind profilers and Doppler radar observations.

This study suggests that a deterministic forecast of large-amplitude gravity waves is possible with state-of-the-art mesoscale models initialized with conventional surface and rawinsonde data. This is not to say, however, that fully reliable gravity wave predictions can be expected on a routine basis.

#### Acknowledgments

Discussions with Chris Davis, Yuh-Lang Lin, Lance Bosart, Melvin Shapiro, Richard Rotunno and Chris Snyder were very helpful. Thanks are also due to John Nielsen-Gammon and the other anonymous reviewer for their insightful reviews of the early versions of the manuscript. This research was partially supported by the NSF grant ATM0200329.

#### References

- Anthes RA (1977) A cumulus parameterization scheme utilizing a one-dimensional cloud model. *Mon Wea Rev* 105: 270–286
- Bosart LF, Cussen JP Jr (1973) Gravity wave phenomena accompanying east coast cyclogenesis. *Mon Wea Rev* 101: 446–454
- Bosart LF, Sanders F (1986) Mesoscale structure in the megapolitan snowstorm of 11–12 February 1983. Part III: A large amplitude gravity wave. *J Atmos Sci* 43: 924–939

- Bosart LF, Bracken WE, Seimon A (1998) A study of cyclone mesoscale structure with emphasis on a large-amplitude inertia-gravity waves. *Mon Wea Rev* 126: 1497–1527
- Brunk I (1949) The pressure pulsation of 11 April 1944. *J Meteor* 6: 181–187
- Crook NA (1988) Trapping of low-level internal gravity waves. *J Atmos Sci* 45: 1533–1541
- Dudhia J (1993) A nonhydrostatic version of the Penn State-NCAR Mesoscale Model: Validation tests and simulation of an Atlantic cyclone and cold front. *Mon Wea Rev* 121: 1493–1513
- Emanuel KA (1982) Inertial instability and mesoscale convective systems. Part II: Symmetric CISK in a baroclinic flow. *J Atmos Sci* 39: 1080–1097
- Eom JK (1975) Analysis of the internal gravity wave occurrence of 19 April 1970 in the Midwest. *Mon Wea Rev* 103: 217–226
- Ferguson HL (1967) Mathematical and synoptic aspects of a small scale wave disturbance over the Lower Great Lakes area. *J Appl Meteor* 6: 523–529
- Grell GA (1993) Prognostic evaluation of assumptions used by cumulus parameterizations. *Mon Wea Rev* 121: 764–787
- Grell GA, Dudhia J, Stauffer DS (1995) A description of the fifth-generation Penn State/NCAR mesoscale model (MM5). NCAR Technical Note, NCAR/TN-398 + STR, 122 pp
- Hooke WH (1986) Gravity waves. In: *Mesoscale meteorology and forecasting* (Ray PS, ed.), Am Meteor Soc, Boulder, CO, pp 272–288
- Jones WL (1968) Reflection and stability of waves in stably stratified fluids with shear flow: A numerical study. *J Fluid Mech* 34: 609–624
- Kaplan ML, Koch SE, Lin Y-L, Weglarz RP, Rozumalski RA (1997) Numerical simulations of a gravity wave event over CCOPE. Part I: The role of geostrophic adjustment in mesoscale jetlet formation. *Mon Wea Rev* 125: 1185–1211
- Karyampudi VM, Kaplan ML, Koch SE, Zamora R (1995a) The influence of the Rocky Mountains in the 13–14 April 1986 severe weather outbreak. Part I: Mesoscale lee cyclogenesis and its relationship to severe weather outbreak. *Mon Wea Rev* 123: 1394–1422
- Karyampudi VM, Koch SE, Chen C, Rottman JW, Kaplan ML (1995b) The influence of the Rocky Mountain in the 13–14 April 1986 severe weather outbreak. Part II: Evolution of an internal bore and its role in triggering a squall line. *Mon Wea Rev* 123: 1423–1446
- Klemp JB, Durran DR (1983) An upper boundary condition permitting internal gravity wave radiation in numerical mesoscale models. *Mon Wea Rev* 111: 430–444
- Koch SE, Dorian PB (1988) A mesoscale gravity wave event observed during CCOPE. Part III: Wave environment and probable source mechanisms. *Mon Wea Rev* 116: 2570–2592
- Koch SE, Golus RE (1988) A mesoscale gravity wave event observed during CCOPE. Part I: Multiscale statistical analysis of wave characteristics. *Mon Wea Rev* 116: 2527–2544
- Koch SE, O’Handley C (1997) Operational forecasting and detection of mesoscale gravity waves. *Wea Forecast* 12: 253–281
- Koch SE, Hamilton D, Kramer D, Langmaid A (1998) Mesoscale dynamics in the Palm Sunday tornado outbreak. *Mon Wea Rev* 126: 2031–2060
- Koch SE, Wu Y, Jin Y, Zhang F (1999) How predictable are mesoscale gravity waves? Preprints 8th Conf. on Mesoscale Processes, Amer Meteor Soc, Boulder, CO, pp 73–78
- Koch SE, Zhang F, Kaplan ML, Lin Y-L, Weglarz R, Trexler CM (2001) Numerical simulation of a gravity wave event observed during CCOPE. Part 3: Mountain-plain solenoids in the generation of the second wave episode. *Mon Wea Rev* 129: 909–932
- Koppel LL, Bosart LF, Keyser D (2000) A 25-year climatology of large-amplitude hourly surface pressure changes over the conterminous United States. *Mon Wea Rev* 128: 51–68
- Kuo H-L (1994) Further studies of parameterization of influence of moist convection on large-scale flow. *J Atmos Sci* 31: 1232–1240
- Lin Y-L (1987) Two-dimensional response of a stably stratified shear flow to diabatic heating. *J Atmos Sci* 44: 1375–1393
- Lin Y-L, Goff RC (1988) A case study of solitary wave in the atmosphere originating near a region of deep convection. *J Atmos Sci* 45: 194–205
- Lindzen RS (1974) Wave-CISK in the tropics. *J Atmos Sci* 31: 156–179
- Lindzen RS, Tung KK (1976) Banded convective activity and ducted gravity waves. *Mon Wea Rev* 104: 1602–1617
- Manobianco J, Koch S, Karyampudi V, Negri A (1994) The impact of assimilating satellite-derived precipitation rates on numerical simulations of the ERICA IOP 4 cyclone. *Mon Wea Rev* 122: 343–365
- Monserat S, Thorpe AJ (1996) Use of ducting in an observed case of gravity waves. *J Atmos Sci* 53: 1724–1736
- Pecnick MJ, Young JA (1984) Mechanics of a strong subsynoptic gravity wave deduced from satellite and surface observations. *J Atmos Sci* 41: 1850–1862
- Pokrandt PJ, Tripoli GJ, Houghton DD (1996) Processes leading to the formation of mesoscale waves in the midwest cyclone of 15 December 1987. *Mon Wea Rev* 123: 2726–2752
- Powers JG (1997) Numerical model simulation of a mesoscale gravity wave event: sensitivity tests and spectral analysis. *Mon Wea Rev* 124: 1838–1869
- Powers JG, Reed RJ (1993) Numerical model simulation of the large-amplitude mesoscale gravity-wave event of 15 December 1987 in the central United States. *Mon Wea Rev* 121: 2285–2308
- Ralph FM, Crochet M, Venkateswaran SV (1993a) Observations of a mesoscale ducted gravity wave. *J Atmos Sci* 50: 3277–3291
- Ralph FM, Mazaudier C, Crochet M, Venkateswaran SV (1993b) Doppler sodar and radar wind-profiler observations of gravity-wave activity associated with a gravity current. *Mon Wea Rev* 121: 444–463

- Raymond DJ (1975) A model for predicting the movement of continuously propagating convective storms. *J Atmos Sci* 32: 1308–1317
- Raymond DJ (1984) A wave-CISK model of squall lines. *J Atmos Sci* 41: 1946–1958
- Reisner J, Rasmussen RJ, Bruintjes RT (1998) Explicit forecasting of supercooled liquid water in winter storms using the MM5 mesoscale model. *Quart J Roy Met Soc* 124B: 1071–1107
- Schmidt JW, Cotton WR (1990) Interactions between upper and lower tropospheric gravity waves and squall line structure and maintenance. *J Atmos Sci* 47: 1205–1222
- Schneider RS (1990) Large-amplitude mesoscale wave disturbances within the intense midwest extratropical cyclone of 15 December 1987. *Wea Forecast* 5: 533–558
- Shen B-W, Lin Y-L (1999) Effects of critical levels on two-dimensional back-shear flow over an isolated mountain ridge on an  $f$  plane. *J Atmos Sci* 56: 3286–3302
- Stobie JG, Einaudi F, Uccellini LW (1983) A case study of gravity waves-convective interaction: 9 May 1979. *J Atmos Sci* 40: 2804–2830
- Tepper M (1954) Pressure jump lines in midwestern United States, January–August 1951. Research Paper No. 37, U. S. Weather Bureau, 70 pp
- Uccellini LW (1975) A case study of apparent gravity wave initiation of severe convection storms. *Mon Wea Rev* 103: 497–513
- Uccellini LW, Koch SE (1987) The synoptic setting and possible source mechanisms for mesoscale gravity wave events. *Mon Wea Rev* 115: 721–729
- Wang T-A, Lin Y-L (1999) Wave ducting in a stratified shear flow over a two-dimensional mountain. Part I: General linear criteria. *J Atmos Sci* 56: 412–436
- Zhang D-L, Anthes RA (1982) A high-resolution model of the planetary boundary layer: Sensitivity tests and comparison with SESAME-79 data. *J Appl Meteor* 21: 1594–1609
- Zhang D-L, Fritsch JM (1988) Numerical simulation of the meso-beta scale structure and evolution of the 1977 Johnstown flood. Part III: Internal gravity waves and the squall line. *J Atmos Sci* 45: 1252–1268
- Zhang F (2000) Unbalanced dynamics and topography in the generation of mesoscale gravity waves. Ph.D. Diss. North Carolina State University, 311 pp
- Zhang F, Koch SE (2000) Numerical simulations of a gravity wave event over CCOPE. Part II: Waves generated by an orographic density current. *Mon Wea Rev* 128: 2777–2796
- Zhang F, Koch SE, Davis CA, Kaplan ML, Lin Y-L (2001) Wavelet analysis and the governing dynamics of a large-amplitude mesoscale gravity wave event along the East Coast of the United States. *Quart J Roy Met Soc* 127: 2209–2245

Corresponding author's address: Dr. Fuqing Zhang, Department of Atmospheric Sciences, Texas A&M University, College Station, TX 77843-3150, USA (E-mail: fzhang@tamu.edu)